Clemson University
College of Engineering and Science
Control and Robotics (CRB) Technical Report

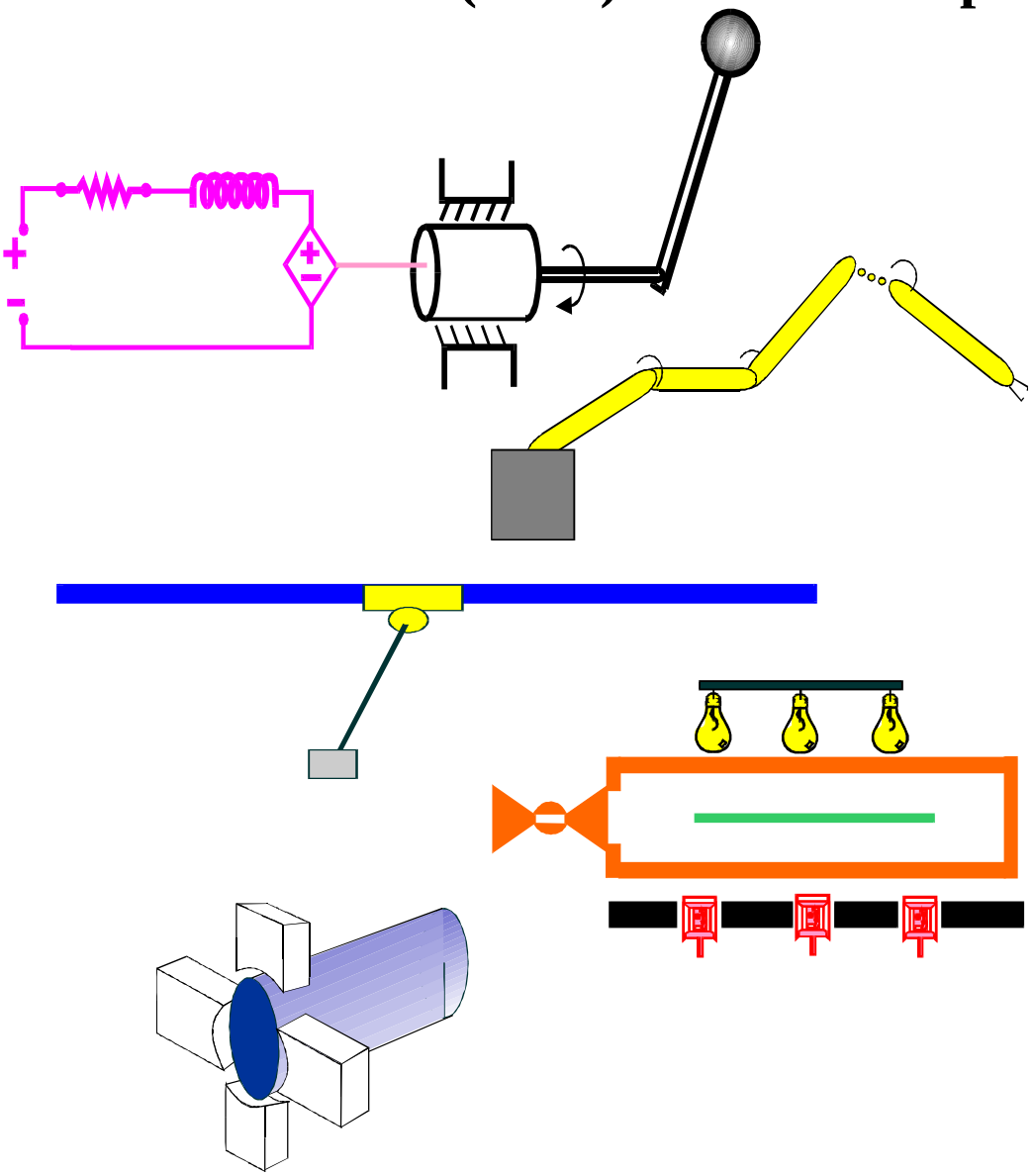

Number: CU/CRB/8/8/05/#1

Title: Vision Assisted Landing of an Unmanned Aerial Vehicle.

Authors: V. K. Chitrakaran, D. M. Dawson, J. Chen and M. Feemster

Report Documentation Page

Form Approved
OMB No. 0704-0188

1. REPORT DATE	2. REPORT TYPE	3. DATES COVERED
2005		**00-00-2005 to 00-00-2005**

4. TITLE AND SUBTITLE	5a. CONTRACT NUMBER
Vision Assisted Autonomous Landing of an Unmanned Aerial Vehicle	5b. GRANT NUMBER
	5c. PROGRAM ELEMENT NUMBER
6. AUTHOR(S)	5d. PROJECT NUMBER
	5e. TASK NUMBER
	5f. WORK UNIT NUMBER
7. PERFORMING ORGANIZATION NAME(S) AND ADDRESS(ES) **Clemson University,Department of Electrical & Computer Engineering,Clemson,SC,29634-0915**	8. PERFORMING ORGANIZATION REPORT NUMBER
9. SPONSORING/MONITORING AGENCY NAME(S) AND ADDRESS(ES)	10. SPONSOR/MONITOR'S ACRONYM(S)
	11. SPONSOR/MONITOR'S REPORT NUMBER(S)

12. DISTRIBUTION/AVAILABILITY STATEMENT
Approved for public release; distribution unlimited

13. SUPPLEMENTARY NOTES
The original document contains color images.

14. ABSTRACT

15. SUBJECT TERMS

16. SECURITY CLASSIFICATION OF:			17. LIMITATION OF ABSTRACT	18. NUMBER OF PAGES	19a. NAME OF RESPONSIBLE PERSON
a. REPORT	b. ABSTRACT	c. THIS PAGE			
unclassified	**unclassified**	**unclassified**		**8**	

Vision Assisted Autonomous Landing of an Unmanned Aerial Vehicle.[1]

Vilas K. Chitrakaran[†], Darren M. Dawson[†], Jian Chen[†] and Mathew Feemster[‡]

[†]Department of Electrical & Computer Engineering, Clemson University, Clemson, SC 29634-0915

[‡]Weapons and Systems Engineering Department, U.S. Naval Academy, Annapolis, MD 21402-5000

E-mail: cvilas@ces.clemson.edu, jian.chen@ieee.org, ddawson@ces.clemson.edu, feemster@usna.edu

Abstract

In this paper, a strategy for an autonomous landing maneuver for an underactuated, unmanned aerial vehicle (UAV) using position information obtained from a single monocular on-board camera is presented. Although the UAV is underactuated in translational control inputs (i.e., a lift force can only be produced), the proposed controller is shown to achieve globally uniform ultimate boundedness (GUUB) in position regulation error during the landing approach. The proposed vision-based control algorithm is built upon homography-based techniques and Lyapunov design methods.

1 Introduction

Underactuated autonomous vehicles such as underwater vehicles, aircrafts, and helicopters are typically equipped with a lower number of control inputs than degrees of freedom to reduce factors such as weight, complexity, and power consumption. As a result, these vehicles may not be fully equipped with sufficient translational actuators that allow for independent translation along any given direction. Hence, the control design for these underactuated vehicles are complicated due to the fact that the rotational torques must be coupled with the translational system in order to achieve the overall position objective.

In addition to the challenges involved in the design of a control strategy for underactuated dynamic systems, there exists the problem of accurate position measurement in such machines. Flying machines are usually equipped with on-board inertial sensors which only measure the rate of motion. The position information is thus obtained from time integration of rate data, resulting in potential drift over time due to sensor noise. To overcome this problem, the use of a vision sensor and computer vision techniques within the feedback loop of such systems is becoming increasingly attractive, due to their ever decreasing size and cost of implementation relative to the computing power required for processing the visual data. Performance analysis of a visual sensor in the feedback loop has been reported in great detail in [10], where visual data was utilized for the estimation of position and velocity of a helicopter during a landing procedure. Experimental results of this approach were subsequently published in [11]. In addition, simulation results for the dynamic control of the X4 flyer based on visual feedback was presented in [13].

In this paper, a single calibrated monocular camera is utilized as a feedback sensor within a position regulation control scheme for an unmanned aerial vehicle (UAV) during a landing maneuver. The UAV is assumed to be equipped with Inertial Navigation Sensors (INS) from which velocity information can be calculated. A homography-based approach, described in [12] and reported in such visual servoing related works as [2] and [14] has been utilized for the determination of the position and orientation of the UAV with respect to the landing pad. The homography-based approach is well suited for this application, since all visual markers are embedded on a flat planar landing pad. Similar to the approach followed in [1], a constant design vector is integrated within the filtered regulation error signal, resulting in an input matrix that facilitates an advantageous coupling of translational dynamics of the UAV to the rotational torque inputs. Additionally, the null space of this input matrix is exploited to achieve a secondary control objective of damping the orientation error signal of the UAV to within a neighborhood about zero which can be made arbitrarily small through the proper selection of design parameters (*i.e.*, global uniform ultimate boundedness (GUUB)).

The remainder of the paper is organized in the following manner. In Section 2, the geometric relationship between the coordinate frames of the UAV and the landing pad are expressed in terms of a sequence of images of the landing pad acquired from an on-board camera. A simplified dynamic model of a rigid body, underactuated UAV is subsequently presented in Section 2.2. The problem formulation, assumptions, and position regulation control objective are presented in Section 3. The control development, based on the rigid body dynamics and the position error information determined from the vision system, are provided in Section 4 along with a Lyapunov based stability analysis. Conclusions are presented in Section 5.

2 System Model

2.1 Vision System and Geometric Model

In order to obtain accurate position information, an aerial vehicle is outfitted with an on-board camera such that the optical axis is coincident with the vertical axis of the UAV body fixed frame, denoted by $\mathcal{B}$. The landing surface, denoted by π, is augmented with many stationary, coplanar visual markers O_i, all of them assumed to be in the

[1]This work was supported in part by two DOC Grants, an ARO Automotive Center Grant, a DOE Contract, a Honda Corporation Grant, and a DARPA Contract.

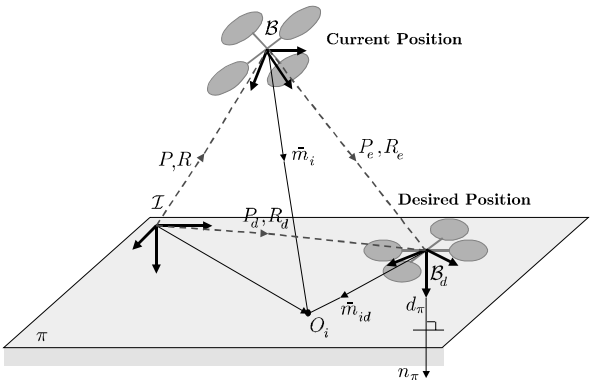

Figure 1: The relationship between inertial and body fixed coordinate frames for a UAV on a landing approach.

field of view of the camera throughout the entire landing approach. The Euclidean position of the UAV with respect to the inertial frame $\mathcal{I}$ is represented by $P(t) \in \mathbb{R}^3$, and the orientation of the UAV $\mathcal{B}$ is expressed through the rotational matrix $R(t) \in SO(3)$ where $R(t)$ represents the mapping $R : \mathcal{B} \to \mathcal{I}$. $\mathcal{B}_d$ represents the desired landing orientation of the UAV, $P_d \in \mathbb{R}^3$ denotes the desired, constant position vector, and $R_d \in SO(3)$ denotes the constant orthogonal rotation matrix with the following mapping characteristics $R_d : \mathcal{B}_d \to \mathcal{I}$. As shown in Figure 1, the translation and rotation of the frame $\mathcal{B}_d$ relative to $\mathcal{B}$ is quantified by $P_e(t) \in \mathbb{R}^3$ and $R_e(t) \in SO(3)$, respectively, where R_e represents the mapping $R_e : \mathcal{B}_d \to \mathcal{B}$.

Let $\bar{m}_i(t), \bar{m}_{id} \in \mathbb{R}^3$ denote the Euclidean coordinates of the i^{th} visual marker O_i on the landing surface relative to the camera at position $\mathcal{B}$ and $\mathcal{B}_d$, respectively. From the geometry between the coordinate frames, $\bar{m}_i(t)$ and $\bar{m}_{id}$ are related as follows

$$\bar{m}_i = P_e + R_e \bar{m}_{id}. \tag{1}$$

Also illustrated in Figure 1, $n_\pi \in \mathbb{R}^3$ denotes the known constant normal to the plane π expressed in the coordinates of $\mathcal{B}_d$, and the constant $d_\pi \neq 0 \in \mathbb{R}$ denotes the distance of the landing surface π from the origin of the frame $\mathcal{B}_d$. It can be seen from Figure 1 that for all i visual markers, the projection of $\bar{m}_{id}$ along the unit normal n_π is given by

$$d_\pi = n_\pi^T \bar{m}_{id}. \tag{2}$$

Using (2), the relationship in equation (1) can be expressed in the following manner

$$\bar{m}_i = \underbrace{\left(R_e + \frac{1}{d_\pi} P_e n_\pi^T\right)}_{H} \bar{m}_{id} \tag{3}$$

where $H(t) \in \mathbb{R}^{3\times 3}$ represents a Euclidean Homography [12]. To express the above relationship in terms of the measurable image space coordinates of the visual markers relative to the camera frame, the normalized Euclidean coordinates $m_i(t), m_{id} \in \mathbb{R}^3$ for the visual markers are defined as

$$m_i \triangleq \frac{\bar{m}_i}{z_i}, \qquad m_{id} \triangleq \frac{\bar{m}_{id}}{z_{id}} \tag{4}$$

where $z_i(t)$ and z_{id} are the third coordinate elements in the vectors $\bar{m}_i(t)$ and $\bar{m}_{id}$, respectively. The 2D homogeneous image coordinates of the visual markers, denoted by $p_i(t), p_{id} \in \mathbb{R}^3$, expressed relative to $\mathcal{B}$ and $\mathcal{B}_d$, respectively, are related to the normalized Euclidean coordinates by the pin-hole model of [4] such that

$$p_i = A m_i, \qquad p_{id} = A m_{id} \tag{5}$$

where $A \in \mathbb{R}^{3\times 3}$ is a known, constant, upper triangular and invertible intrinsic camera calibration matrix [14]. Hence the relationship in (3) can now be expressed in terms of image coordinates of the corresponding feature points in $\mathcal{B}$ and $\mathcal{B}_d$ as follows

$$p_i = \underbrace{\frac{z_{id}}{z_i}}_{\alpha_i} \underbrace{A\left(R_e + \frac{1}{d_\pi} P_e {n_\pi}^T\right) A^{-1}}_{G} p_{id} \tag{6}$$

where $\alpha_i(t) \in \mathbb{R}$ denotes the depth ratio. The matrix $G(t) \in \mathbb{R}^{3\times 3}$ in (6) is a full rank homogeneous collineation matrix defined up to a scale factor [14], and contains the motion parameters $P_e(t)$ and $R_e(t)$ between the frames $\mathcal{B}$ and $\mathcal{B}_d$.

Given pairs of image correspondences $(p_i(t), p_{id})$ for four feature points O_i, at least three of which are non-collinear, the set of linear equations in (6) can be solved to compute a unique $G(t)$ up to a scale factor [12]. When more than four feature point correspondences are available, $G(t)$ can also be recovered (again, up to a scale factor) using techniques such as least-squares minimization. $G(t)$ can then be used to uniquely determine $H(t)$, taking into account its known structure to eliminate the scale factor, and the fact that the intrinsic camera calibration matrix A is assumed to be known [12]. By utilizing various techniques (*e.g.*, see [5, 12, 16]), $H(t)$ can be decomposed to recover the rotational component $R_e(t)$ and the scaled translational component $\frac{1}{d_\pi} P_e(t)$; therefore, $R_e(t)$ and $\frac{1}{d_\pi} P_e(t)$ are assumed to be measurable during the subsequent control development.

2.2 Dynamic Model of a UAV

In this paper, a UAV that is fully actuated with respect to orientation but underactuated with respect to translation is considered (*i.e.*, the UAV is equipped with only one control input (the thrust force) to facilitate translational motion). The control development is focused on the rigid body dynamics of the UAV. That is, actuator dynamics are not considered within the scope of the design. After denoting $v(t), \omega(t) \in \mathbb{R}^3$ as the translational and rotational velocities of the UAV relative to the inertial frame $\mathcal{I}$ expressed in the body frame $\mathcal{B}$, the rigid body dynamics can be described by the following equations [13]

$$\dot{P} = Rv \tag{7}$$

$$m\dot{v} = -mS(\omega)v + N_1(\cdot) + F_f \tag{8}$$

$$\dot{R} = RS(\omega) \tag{9}$$

$$J\dot{\omega} = -S(\omega)J\omega + N_2(\cdot) + F_t \tag{10}$$

where $S(\cdot) \in \mathbb{R}^{3\times 3}$ denotes a skew-symmetric matrix defined in [15], $J \in \mathbb{R}^{3\times 3}$ denotes the constant moment of inertia around the center of mass expressed in body frame $\mathcal{B}$, and $m \in \mathbb{R}^1$ represents the constant mass of the UAV. The term $N_1(P, v, R, t) \in \mathbb{R}^3$ represents the sum of gravitational

forces and additional time varying unmodeled bounded dynamics such as aerodynamic resistance. Similarly, the term $N_2(P, v, R, \omega, t) \in \mathbb{R}^3$ include unmodeled, bounded disturbances within the rotational dynamics. The forces and torques on the rigid body due to the actuators are denoted by $F_f(t), F_t(t) \in \mathbb{R}^3$, respectively, expressed in the body frame $\mathcal{B}$, and given as follows

$$F_f = B_1 u_1 \tag{11}$$

$$F_t = \begin{bmatrix} u_2 & u_3 & u_4 \end{bmatrix}^T \tag{12}$$

where $u_1(t) \in \mathbb{R}^1$ denotes the magnitude of the thrust force and $B_1 = \begin{bmatrix} 0 & 0 & 1 \end{bmatrix}^T \in \mathbb{R}^3$ is a constant unit vector in the body fixed frame $\mathcal{B}$ in the direction of the thrust force. The force and torque inputs $\begin{bmatrix} u_1(t) & u_2(t) & u_3(t) & u_4(t) \end{bmatrix}^T \in \mathbb{R}^4$ are related to the corresponding actuator control signals through dynamics that not considered within the scope of this control design. For example, the four rotor velocities $\varpi_i \in \mathbb{R}^1$ for a Quad-Rotor UAV are related to the rigid body forces and torques via the following relationship [6]

$$\begin{bmatrix} u_1 \\ u_2 \\ u_3 \\ u_4 \end{bmatrix} = \begin{bmatrix} -b & -b & -b & -b \\ 0 & db & 0 & -db \\ db & 0 & -db & 0 \\ k & -k & k & -k \end{bmatrix} \begin{bmatrix} \varpi_1^2 \\ \varpi_2^2 \\ \varpi_3^2 \\ \varpi_4^2 \end{bmatrix} \tag{13}$$

where $d \in \mathbb{R}^1$ denotes the displacement of each rotor relative to the center of mass of the airframe, and $k, b \in \mathbb{R}^1$ are constant parameters that depend on construction and aerodynamic properties of the rotor blades.

3 Problem Formulation

The control design is developed under the assumptions that the translational and rotational velocity signals $v(t)$ and $\omega(t)$, are measurable via on-board sensors and that the UAV mass m and the UAV inertia matrix J are assumed to be known. In addition, the desired position and orientation at landing, defined by P_d and R_d, respectively, are specified. The overall objective is to design the control inputs $F_f(t)$ and $F_t(t)$ to regulate the UAV position $P(t)$ to the desired landing position P_d. Since the UAV has only one translational actuator oriented along a fixed direction defined by the vector B_1, the force input signal $F_f(t)$ must be designed in conjunction with the torque input vector $F_t(t)$ to achieve the desired objective. To this end, the position regulation error signal $e_p(t) \in \mathbb{R}^3$ is defined to quantify the mismatch between the desired and actual position of the UAV as given by

$$e_p \triangleq \frac{1}{d_\pi} R^T (P - P_d) = -\frac{1}{d_\pi} P_e \tag{14}$$

where the fact that $P_d = P + RP_e$ has been utilized.

In addition, it is assumed that a reference image (defined by image coordinates p_{id}) of all visual markers from the on-board camera when the UAV is at the desired landing configuration defined by P_d and R_d, and denoted by $\mathcal{B}_d$ is available. As discussed in Section 2.1, the stereo-like imaging technique allows us to compute the scaled position $\frac{1}{d_\pi} P_e(t)$ and orientation $R_e(t)$ of the UAV relative to the frame $\mathcal{B}_d$ from a sequence of images from the camera on board.

Remark 1 *Since the desired landing configuration defined by P_d and R_d, and the normal vector to the landing surface n_π are assumed to be known, the distance d_π can be computed in the following manner*

$$d_\pi = -n_\pi^T R_d^T P_d. \tag{15}$$

Hence, the scale ambiguity in $\frac{1}{d_\pi} P_e(t)$ from the decomposition of homography can be resolved resulting in calculation of $P_e(t)$. This allows for the computation of the time varying position $P(t)$ and orientation $R(t)$ of the UAV as follows

$$R = R_d R_e^T \tag{16}$$

$$P = P_d - RP_e. \tag{17}$$

4 Control Development

After taking the time derivative of (14), and using (7) and (9), the open loop error dynamics for $e_p(t)$ can be expressed as follows

$$\dot{e}_p = -S(\omega) e_p + \frac{1}{d_\pi} v. \tag{18}$$

To facilitate the regulation of the position error, a filtered regulation error signal $r(t) \in \mathbb{R}^3$ is defined in the following manner

$$r \triangleq v + k_p e_p + \delta \tag{19}$$

where $k_p \in \mathbb{R}^1$ denotes a positive, scalar constant, and $\delta = \begin{bmatrix} \delta_1 & \delta_2 & \delta_3 \end{bmatrix}^T \in \mathbb{R}^3$ represents a constant design vector of positive elements that facilitates an advantageous coupling of the translational dynamics of the UAV to both the translational and rotational control inputs. After taking the time derivative of (19), substituting the translational dynamics from (8) and the open loop error dynamics from (18), the open loop dynamics for the filtered regulation error signal $r(t)$ can be developed as follows

$$\begin{aligned} \dot{r} &= \dot{v} + k_p \dot{e}_p \\ &= -S(\omega) r + \left[\frac{1}{m} B_1 u_1 - S(\delta)\omega \right] \\ &\quad + \frac{1}{m} N_1 + \frac{k_p}{d_\pi} v \end{aligned} \tag{20}$$

where the term $S(\omega)\delta$ has been added and subtracted to the right hand side of the above equation and the fact that $S(\omega)\delta = -S(\delta)\omega$ has been utilized. The bracketed terms in the above equation can be written in terms of a constant auxiliary matrix $\bar{B} \in \mathbb{R}^{3\times 4}$ and an auxiliary vector $\bar{U}(t) \in \mathbb{R}^4$ in the following manner

$$\frac{1}{m} B_1 u_1 - S(\delta)\omega = \bar{B}\bar{U} \tag{21}$$

where

$$\bar{B} \triangleq \begin{bmatrix} 0 & 0 & \delta_3 & -\delta_2 \\ 0 & -\delta_3 & 0 & \delta_1 \\ \frac{1}{m} & \delta_2 & -\delta_1 & 0 \end{bmatrix} \tag{22}$$

$$\bar{U} \triangleq \begin{bmatrix} u_1 & \omega_1 & \omega_2 & \omega_3 \end{bmatrix}^T. \tag{23}$$

In order to proceed with the control development, the angular velocity error signal $\eta(t) \in \mathbb{R}^3$ and the desired control signal $\bar{U}_d(t) \in \mathbb{R}^4$ are defined in the following manner

$$\eta \triangleq \omega_d - \omega \tag{24}$$

$$\bar{U}_d \triangleq \begin{bmatrix} u_1 & \omega_d^T \end{bmatrix}^T \tag{25}$$

where $\omega_d(t) \in \mathbb{R}^3$ represents a desired angular velocity signal. From (23), (24) and (25), the following relationship can be observed

$$\bar{U} = \bar{U}_d - \Pi^T \eta \tag{26}$$

where $\Pi \in \mathbb{R}^{3\times 4}$ denotes the following constant matrix

$$\Pi = \begin{bmatrix} 0 & 1 & 0 & 0 \\ 0 & 0 & 1 & 0 \\ 0 & 0 & 0 & 1 \end{bmatrix}. \tag{27}$$

The desired control input signal $\bar{U}_d(t)$ is designed in the following manner

$$\bar{U}_d = \bar{B}^+ U_{aux} + \left(I_4 - \bar{B}^+ \bar{B}\right) U_{self} \tag{28}$$

where $\bar{B}^+ \triangleq \bar{B}^T \left(\bar{B}\bar{B}^T\right)^{-1} \in \mathbb{R}^{4\times 3}$ denotes the pseudo-inverse of the constant matrix $\bar{B}$, $I_4 \in \mathbb{R}^{4\times 4}$ represents the identity matrix, $U_{aux}(t) \in \mathbb{R}^3$ and $U_{self}(t) \in \mathbb{R}^4$ denote yet to be designed auxiliary control signals. In order for $\bar{B}^+$ to exist, $\bar{B}$ must be of rank 3 which can be easily satisfied through proper selection of the auxiliary matrix δ (*e.g.,* $\delta = \begin{bmatrix} 0 & 0 & \delta_3 \end{bmatrix}^T$ where $\delta_3 \neq 0$).

Since the term $\left(I_4 - \bar{B}^+ \bar{B}\right)$ in (28) projects the vector $U_{self}(t)$ into the null space of $\bar{B}(t)$, the design of $U_{self}(t)$ has no direct influence on the dynamics of $r(t)$. Therefore from (20), (21), (26) and (28), the open loop dynamics for $r(t)$ are given by the following expression

$$\dot{r} = -S(\omega) r + U_{aux} - \bar{B}\Pi^T \eta + \frac{k_p}{d_\pi} v + \bar{N}_1 \tag{29}$$

where, $\bar{N}_1(\cdot) = \frac{1}{m} N_1(\cdot) \in \mathbb{R}^3$, and the following two properties of the pseudo-inverse were employed [9]

$$\begin{aligned} &\bar{B}\bar{B}^+ = I_3 \\ &\bar{B}\left(I_4 - \bar{B}^+ \bar{B}\right) = 0 \end{aligned} \tag{30}$$

where $I_3 \in \mathbb{R}^{3\times 3}$ represents the identity matrix. Since $U_{self}(t)$ does not appear within the dynamics of (29), the auxiliary control input $U_{self}(t)$ can be designed to achieve a secondary control objective, such as the damping of the orientation error of the UAV. To this end, orientation error signal $e_\theta(t) = \begin{bmatrix} e_{\theta 1}(t) & e_{\theta 2}(t) & e_{\theta 3}(t) \end{bmatrix} \in \mathbb{R}^3$ is defined in terms of the axis-angle representation [15] of the orientation matrix $R_e(t)$ in the following manner

$$e_\theta = \mu \phi \tag{31}$$

where $\mu(t) \in \mathbb{R}^3$ represents a unit axis of rotation, $\phi(t) \in \mathbb{R}^1$ denotes the rotation angle about $\mu(t)$ (confined to the region $-\pi < \phi(t) < \pi$) and is explicitly defined in the following manner

$$\phi = \cos^{-1}\left(\frac{1}{2}\left(\text{tr}(R_e) - 1\right)\right) \quad S(\mu) = \frac{R_e - R_e^T}{2\sin(\phi)} \tag{32}$$

where the notation $\text{tr}(\cdot)$ denotes the trace of a matrix. After taking the time derivative of (31), the kinematics of the moving UAV frame is expressed as follows [2]

$$\dot{e}_\theta = -L_\omega \omega \tag{33}$$

where the bounded, invertible, Jacobian like term $L_\omega(t) \in \mathbb{R}^{3\times 3}$ is given by the following expression

$$\begin{aligned} L_\omega &= I_3 - \frac{\phi}{2} S(\mu) + \left(1 - \frac{sinc(\phi)}{sinc^2\left(\frac{\phi}{2}\right)}\right) S(\mu)^2, \\ sinc(\phi) &\triangleq \frac{\sin(\phi)}{\phi}. \end{aligned} \tag{34}$$

For more details on the derivation of (34), the reader is referred to [2]. The kinematics for the UAV can be rewritten in terms of the backstepping velocity error signal $\eta(t)$ and the desired control signal $\bar{U}_d(t)$ in the following manner

$$\dot{e}_\theta = L_\omega \left(\eta - \Pi \bar{U}_d\right). \tag{35}$$

After substituting for $\bar{U}_d(t)$ from (28), $\dot{e}_\theta(t)$ can be rewritten in the following manner

$$\begin{aligned} \dot{e}_\theta &= \left[L_\omega \eta - L_\omega \Pi \bar{B}^+ U_{aux}\right] \\ &\quad -L_\omega \Pi \left(I_4 - \bar{B}^+ \bar{B}\right) U_{self} \\ &= -B_m^T U_{self} + N_3 \end{aligned} \tag{36}$$

where $B_m^T(t) \in \mathbb{R}^{3\times 4}$ is a bounded, differentiable matrix defined as follows

$$B_m^T = L_\omega \Pi \left(I_4 - \bar{B}^+ \bar{B}\right) \tag{37}$$

and the bracketed terms in (36) have been redefined by the single term $N_3(\cdot) \in \mathbb{R}^3$.

Based on the subsequent stability analysis, the control signals $U_{aux}(t)$ and $U_{self}(t)$ are designed as follows

$$U_{aux} = -e_p - k_r r - \frac{k_p}{d_\pi} v - r\frac{\zeta_1^2}{\varepsilon_1} \tag{38}$$

$$U_{self} = k_\theta B_m \text{Tanh}(e_\theta) \tag{39}$$

where $k_r, k_\theta \in \mathbb{R}^1$ are positive, scalar control gains chosen such that $k_p > k_r > 0$, $\varepsilon_1 \in \mathbb{R}^1$ is a positive, scalar constant, $\text{Tanh}(e_\theta) \in \mathbb{R}^3$ is a vector function defined in the following manner

$$\text{Tanh}(e_\theta) = \begin{bmatrix} \tanh(e_{\theta 1}) & \tanh(e_{\theta 2}) & \tanh(e_{\theta 3}) \end{bmatrix}^T \tag{40}$$

and $\zeta_1(\cdot) \in \mathbb{R}^1$ is a known positive, scalar, differentiable, non-decreasing bounding function selected such that

$$\left\|\bar{N}_1\right\| \leq \zeta_1\left(\|P\|_s, \|v\|_s\right) \tag{41}$$

and the function $\|.\|_s$ is defined in the following manner

$$\|y\|_s \triangleq \sqrt{y^T y + \sigma}, \ \forall y \in \mathbb{R}^3 \tag{42}$$

where $\sigma \in \mathbb{R}^1$ represents a small positive constant.

Remark 2 *The function in (42) has been utilized instead of the standard Euclidean norm to ensure that the time derivative of $\zeta_1(\cdot)$ in (41) is well-defined. The time derivative of $\|.\|_s$ is expressed as follows*

$$\frac{d}{dt}\|y\|_s = \frac{y^T \dot{y}}{\sqrt{y^T y + \sigma}}, \ \forall y \in \mathbb{R}^3. \tag{43}$$

Remark 3 *The subsequent stability analysis will require that $U_{self}(t) \in \mathcal{L}_\infty$ be independent of the boundedness of $e_\theta(t)$ thus motivating the design of $U_{self}(t)$ in terms of Tanh(e_θ).*

The control force input $F_f(t)$ can be obtained from $\bar{U}_d(t)$ in (28) as follows

$$F_f = B_2 \bar{U}_d \tag{44}$$

where $B_2 \in \mathbb{R}^{3\times 4}$ is a constant matrix defined as follows

$$B_2 = \begin{bmatrix} 0 & 0 & 0 & 0 \\ 0 & 0 & 0 & 0 \\ 1 & 0 & 0 & 0 \end{bmatrix}.$$

In order to design the control torque input $F_t(t)$, the open-loop dynamics of $\eta(t)$ are formulated by differentiating (24) and substituting the rotational dynamics given in (10) as follows

$$J\dot{\eta} = J\dot{\omega}_d + S(\omega)J\omega - N_2 - F_t. \tag{45}$$

The signal $\dot{\omega}_d(t)$ of (45) is computed from the time derivative of $\bar{U}_d(t)$ in (28); moreover the resulting expression can be written as a sum of two terms $\dot{\bar{U}}_{d1}(t) \in \mathbb{R}^4$ and $\dot{\bar{U}}_{d2}(t) \in \mathbb{R}^4$, where $\dot{\bar{U}}_{d1}(t)$ is composed of the known terms of $\dot{\bar{U}}(t)$, and $\dot{\bar{U}}_{d2}(t)$ is composed of uncertain terms (see the Appendix for explicit forms of $\dot{\bar{U}}_{d1}(t)$ and $\dot{\bar{U}}_{d2}(t)$). Hence, (45) can be rewritten as

$$J\dot{\eta} = J\Pi\dot{\bar{U}}_{d1} + S(\omega)J\omega - \bar{N}_2 - F_t \tag{46}$$

where the uncertain terms have been lumped into a single term $\bar{N}_2(t) \in \mathbb{R}^3$ which is defined as follows

$$\bar{N}_2 = N_2 - J\Pi\dot{\bar{U}}_{d2}. \tag{47}$$

Based on the subsequent stability analysis, the control torque input $F_t(t)$ is designed in the following manner

$$F_t = J\Pi\dot{\bar{U}}_{d1} + S(\omega)J\omega + k_r\eta - \Pi\bar{B}^T r + \eta\frac{\zeta_2^2}{\varepsilon_2} \tag{48}$$

where $\varepsilon_2 \in \mathbb{R}^1$ represents a positive, scalar constant, and $\zeta_2(\cdot) \in \mathbb{R}^1$ is a known positive, scalar, non-decreasing bounding function constructed such that

$$\left\|\bar{N}_2\right\| \le \zeta_2\left(\|P\|, \|v\|, \|\omega\|\right). \tag{49}$$

4.1 Stability Analysis

Theorem 1 *Given the error dynamics of (18), (29) and (45), the translational force input and the rotational torque input developed in (44) and (48), respectively, guarantees that the position error signal $e_p(t)$ is exponentially regulated into a neighborhood about zero (GUUB)*

$$\|e_p(t)\| \le \alpha_1 \exp\left(-\alpha_2 t\right) + \alpha_3 \tag{50}$$

where $\alpha_1, \alpha_2, \alpha_3 \in \mathbb{R}^1$ are adjustable, positive constants.

Proof: In order to illustrate the position regulation result of (50), the following non-negative scalar function is defined

$$V \triangleq \frac{1}{2}d_\pi e_p^T e_p + \frac{1}{2}r^T r + \frac{1}{2}\eta^T J\eta. \tag{51}$$

After taking the time derivative of (51), substituting the dynamics for $\dot{e}_p(t), \dot{r}(t)$ and $\dot{\eta}(t)$ from (18), (29) and (45), and substituting the expressions for $U_{aux}(t)$ and $F_t(t)$ from (38) and (48), the time derivative for $V(t)$ can be expressed in the following manner

$$\begin{aligned} \dot{V} \le & -k_r\|e_p\|^2 - k_r\|r\|^2 - k_r\|\eta\|^2 \\ & + \left[\|r\|\zeta_1 - \frac{\|r\|^2\zeta_1^2}{\varepsilon_1}\right] \\ & + \left[\|\eta\|\zeta_2 - \frac{\|\eta\|^2\zeta_2^2}{\varepsilon_2}\right] \\ & + \left[\|e_p\|\|\delta\| - k\|e_p\|^2\right] \end{aligned} \tag{52}$$

where $k = k_p - k_r \in \mathbb{R}^1$ is a positive constant (recall that the control gain k_r in (38) is selected such that $k_p > k_r > 0$). After applying the nonlinear damping argument from [8], each of the bracketed terms in the above expression can be upper-bounded as follows

$$\begin{aligned} \|r\|\zeta_1\left(1 - \frac{\|r\|\zeta_1}{\varepsilon_1}\right) &\le \varepsilon_1 \\ \|\eta\|\zeta_2\left(1 - \frac{\|\eta\|\zeta_2}{\varepsilon_2}\right) &\le \varepsilon_2 \\ \|e_p\|\left(\|\delta\| - k\|e_p\|\right) &\le \frac{\|\delta\|^2}{k} \end{aligned} \tag{53}$$

From (52), $\dot{V}(t)$ can be further upper bounded in the following manner

$$\dot{V} \le -k_r\|z\|^2 + \varepsilon \tag{54}$$

where $z \triangleq \begin{bmatrix} e_p^T & r^T & \eta^T \end{bmatrix}^T \in \mathbb{R}^9$ and $\varepsilon \triangleq \varepsilon_1 + \varepsilon_2 + \frac{\|\delta\|^2}{k} \in \mathbb{R}^1$. Note that $V(t)$ in (51) satisfies the following inequality

$$\beta_{11}\|z(t)\|^2 \le V(t) \le \beta_{12}\|z(t)\|^2 \tag{55}$$

where the constant parameters $\beta_{11}, \beta_{12} \in \mathbb{R}^1$ are given by

$$\beta_{11} = \min\left(\frac{1}{2}, \lambda_{\min}(J)\right), \beta_{12} = \max\left(\frac{1}{2}, \lambda_{\max}(J)\right) \tag{56}$$

and $\lambda_{\min}(J), \lambda_{\max}(J) \in \mathbb{R}^1$ denote the minimum and maximum eigenvalues of the inertia matrix J, respectively. From (51), (54) and (55), the position error signal $e_p(t)$ can be upperbounded by the following

$$\|e_p(t)\| \le V(t) \le \alpha_1 \exp(-\alpha_2 t) + \alpha_3 \tag{57}$$

where $\alpha_1 = V(0)$, $\alpha_2 = \frac{k_r}{\beta_{12}}$, and $\alpha_3 = \frac{\varepsilon}{\alpha_2}$ are positive scalar constants.

From (54) and (55), it is straightforward to see that $e_p(t), r(t), \eta(t) \in \mathcal{L}_\infty$. Since $R(t) \in \mathcal{L}_\infty$ and $P_d \in \mathcal{L}_\infty$, we can conclude that $P(t) \in \mathcal{L}_\infty$ based on the position error signal definition of (14). From (19), we observe that $v(t) \in \mathcal{L}_\infty$, hence, $U_{aux}(t) \in \mathcal{L}_\infty$. Based on the fact that $e_p(t)$ and $v(t)$ are bounded, we can use (18) to show that $\dot{e}_p(t) \in \mathcal{L}_\infty$. After utilizing (20), (28) and (29), we can determine that $\dot{r}(t), \dot{v}(t) \in \mathcal{L}_\infty$, and hence, $\dot{U}_{aux}(t) \in \mathcal{L}_\infty$. Since $U_{self}(t)$ was designed to be bounded through the utilization of Tanh$(\cdot)$, it can be shown from (28) that $\bar{U}_d(t) \in \mathcal{L}_\infty$, and hence, $\omega_d(t), \bar{U}(t), u_1(t), \omega(t) \in \mathcal{L}_\infty$. Based on the time derivative of $U_{self}(t)$ in the Appendix, we observe that $\dot{U}_{self}(t) \in \mathcal{L}_\infty$. Hence $\dot{\bar{U}}_d(t) \in \mathcal{L}_\infty$, and therefore, it can be shown that $\dot{\omega}_d(t), F_t(t), \dot{\omega}(t), \dot{\eta}(t) \in \mathcal{L}_\infty$. From the preceding stability trace, we can conclude that $F_f(t) \in \mathcal{L}_\infty$ from

(44). Therefore, all signals remain bounded during closed loop operation. ■

Remark 4 *With $U_{self}(t)$ designed as shown in (39), the expression of (36) can now be written as follows*

$$\dot{e}_\theta = -k_\theta B_m^T B_m Tanh\left(e_\theta\right) + N_3 \tag{58}$$

It is apparent from (58) that $U_{self}(t)$ has been designed to damp the orientation error signal $e_\theta(t)$, since Theorem 1 has illustrated that $N_3(\cdot) \in \mathcal{L}_\infty$.

5 Conclusions

In this paper, a nonlinear controller was developed to achieve position regulation of a rigid, underactuated aerial vehicle during a landing approach using position information obtained from an on-board monocular camera. The controller was shown to achieve globally uniform ultimate boundedness (GUUB) in position regulation error despite uncertain bounded disturbances in the system dynamics. Additionally, the null space of an input matrix in the controller was exploited to achieve a secondary control objective of damping the orientation error of the UAV relative to the desired orientation at landing.

References

[1] A. Aguiar, and J. Hespanha, "Position Tracking of Underactuated Vehicles," *Proceedings of the American Control Conference*, pp. 1988-1993, Denver, CO, June 2003.

[2] J. Chen, D. M. Dawson, W. E. Dixon, and A. Behal,"Adaptive Homography-Based Visual Servo Tracking for Fixed and Camera-in-Hand Configurations," *IEEE Transactions on Control System Technology*, to appear.

[3] V. K. Chitrakaran, D. M. Dawson, J. Chen, and M. Feemster, "Vision Assisted Landing of an Unmanned Aerial Vehicle," Clemson University CRB Technical Report, CU/CRB/8/8/05/#1, http://www.ces.clemson.edu/ece/crb/publictn/tr.htm, Aug. 2005.

[4] O. Faugeras, *Three-Dimensional Computer Vision*, The MIT Press, ISBN: 0262061589, 1993.

[5] O. Faugeras, and F. Lustman, "Motion and Structure From Motion in a Piecewise Planar Environment," *International Journal of Pattern Recognition and Artificial Intelligence*, Vol. 2, No. 3, pp. 485–508, 1988.

[6] T. Hamel, R. Mahony, R. Lozano, and J. Ostrowski, "Dynamic Modelling and Configuration Stabilization for an X-4 Flyer," *Proceedings of the IFAC World Congress*, Barcelona, Spain, July 2002.

[7] R. Horn, and C. Johnson, *Matrix Analysis*, Cambridge University Press, ISBN: 0521305861, 1985.

[8] M. Krstić, I. Kanellakopoulos, and P. Kokotović, *Nonlinear and Adaptive Control Design*, New York, NY: John Wiley and Sons, 1995.

[9] Y. Nakamura, *Advanced Robotics: Redundancy and Optimization*, Addison-Wesley, ISBN: 0201151987, 1991.

[10] O. Shakernia, Y. Ma, T. J. Koo, and S. Sastry, "Landing an Unmanned Air Vehicle: Vision Based Motion Estimation and Nonlinear Control," *Asian Journal of Control*, Vol. 1, No. 3, pp. 128–145, 1999.

[11] C. Sharp, O. Shakernia, and S. Sastry, "A Vision System for Landing of an Unmanned Aerial Vehicle," *Proceedings of the International Conference on Robotics and Automation*, Vol. 2, 2001, pp. 1720 - 1727.

[12] Y. Ma, S. Soatto, J. Košecká, and S. Sastry, *An Invitation to 3D Vision*, Springer-Verlag, ISBN: 0387008934, 2003.

[13] D. Suter, T. Hamel, and R. Mahony, "Visual Servo Control Using Homography Estimation for the Stabilization of an X4-Flyer," *Proceedings of the IEEE Conference on Decision and Control*, Las Vegas, NV, 2002, pp. 2872-2877.

[14] E. Malis and F. Chaumette, "2 1/2 D Visual Servoing with Respect to Unknown Objects Through a New Estimation Scheme of Camera Displacement," I*nternational Journal of Computer Vision*, Vol. 37, No. 1, 2000, pp. 79–97.

[15] M. W. Spong, and M. Vidyasagar, *Robot Dynamics and Control*, John Wiley and Sons, ISBN: 047161243, 1989.

[16] Z. Zhang, and A. R. Hanson, "Scaled Euclidean 3D Reconstruction Based on Externally Uncalibrated Cameras," *IEEE Symposium on Computer Vision*, 1995, pp. 37–42.

Appendix A: Time Derivative of $\bar{U}_d(t)$

After taking the time derivative of $\bar{U}_d(t)$ in (28), the following expression is obtained

$$\dot{\bar{U}}_d = \bar{B}^+ \dot{U}_{aux} + \left(I_4 - \bar{B}^+ \bar{B}\right) \dot{U}_{self} \tag{59}$$

where the time derivative of $U_{aux}(t)$ can be computed from (38) as follows

$$\begin{aligned} \dot{U}_{aux} &= S(\omega) e_p + \frac{k_p}{d_\pi} S(\omega) v - \frac{1}{d_\pi} v - \frac{k_p}{m d_\pi} B_2 \bar{U}_d \\ &\quad + \left(k_r + \frac{\zeta_1^2}{\varepsilon_1}\right) \left(S(\omega) r - U_{aux} + \bar{B} \Pi^T \eta - \frac{k_p}{d_\pi} v\right) \\ &\quad - \left(k_r + \frac{\zeta_1^2}{\varepsilon_1} + \frac{k_p}{d_\pi}\right) \bar{N}_1 - 2r \frac{\zeta_1}{\varepsilon_1} \dot{\zeta}_1. \end{aligned} \tag{60}$$

The time derivative of $U_{aux}(t)$ can be separated into measurable and unmeasurable bounded terms $\dot{U}_{aux1}(t)$ and $\dot{U}_{aux2}(t)$, respectively, as follows

$$\begin{aligned} \dot{U}_{aux1} &= S(\omega) e_p + \frac{k_p}{d_\pi} S(\omega) v - \frac{1}{d_\pi} v - \frac{k_p}{m d_\pi} B_2 \bar{U}_d \\ &\quad + \left(k_r + \frac{\zeta_1^2}{\varepsilon_1}\right) \left(S(\omega) r - U_{aux} - \frac{k_p}{d_\pi} v \right. \\ &\quad \left. + \bar{B} \Pi^T \eta\right) - 2r \frac{\zeta_1}{\varepsilon_1} \dot{\zeta}_{11} \end{aligned} \tag{61}$$

$$\dot{U}_{aux2} = -\left(k_r \bar{N}_1 + \frac{\zeta_1^2}{\varepsilon_1} \bar{N}_1 + \frac{k_p}{d_\pi} \bar{N}_1 + 2r \frac{\zeta_1}{\varepsilon_1} \dot{\zeta}_{12}\right) \tag{62}$$

where the known and unknown terms in the time derivative of $\zeta_1(\cdot)$ has been separated into $\dot{\zeta}_{11}(\cdot) \in \mathbb{R}^1$ and $\dot{\zeta}_{12}(\cdot) \in \mathbb{R}^1$, respectively. Similarly after taking the time derivative of (39), the time derivative of $U_{self}\left(t\right)$ can be expressed as follows

$$\begin{aligned} \dot{U}_{self} &= B_\theta L_\omega^T \left[I - \right. \\ &\quad \left. diag\left(\tanh^2\left(e_{\theta 1}\right), \tanh^2\left(e_{\theta 2}\right), \tanh^2\left(e_{\theta 3}\right)\right)\right] \dot{e}_\theta \\ &\quad + B_\theta \dot{L}_\omega^T \mathrm{Tanh}\left(e_\theta\right) \end{aligned} \tag{63}$$

where $diag(.)$ denotes a diagonal matrix with arguments as the diagonal entries, the constant matrix $B_\theta \in \mathbb{R}^{4\times 3}$ is defined as

$$B_\theta = k_\theta \left(I_4 - \bar{B}^+ \bar{B}\right)^T \Pi^T \tag{64}$$

and the time derivative of the Jacobian like term $L_\omega(t)$ can be shown to be the following

$$\begin{aligned}\dot{L}_\omega = &= \left\{ \tfrac{1}{4} \left(\frac{\phi - \sin(\phi)}{\sin^2(\frac{\phi}{2})} \right) \mu^T \left(I_3 + S(\mu)^2 \right) \dot{e}_\theta \right\} S(\mu)^2 \\ &+ \left(\frac{sinc\,(\phi)}{sinc^2\left(\frac{\phi}{2}\right)} - 1 \right) \left(\frac{1}{\phi} \mu \dot{e}_\theta^T S(\mu)^2 \right. \\ &\left. + \frac{1}{\phi} S(\mu)^2 \dot{e}_\theta \mu^T \right) - \frac{1}{2} S(\dot{e}_\theta).\end{aligned} \tag{65}$$

The time derivative of $\bar{U}_d(t)$ can now be written as a sum of a measurable $\dot{\bar{U}}_{d1}(t) \in \mathbb{R}^4$ and an unmeasurable $\dot{\bar{U}}_{d2}(t) \in \mathbb{R}^4$ term each defined in the following manner

$$\dot{\bar{U}}_{d1} = \bar{B}^+ \dot{U}_{aux1} + \left(I_4 - \bar{B}^+ \bar{B} \right) \dot{U}_{self} \tag{66}$$

$$\dot{\bar{U}}_{d2} = \bar{B}^+ \dot{U}_{aux2}. \tag{67}$$